Mll4 regulates postnatal palate growth and midpalatal suture development

Jung-Mi Lee[1,*], Hunmin Jung[1], Bruno de Paula Machado Pasqua[1], Yungki Park[2], Shin Jeon[3,4], Soo-Kyung Lee[4], Jae W. Lee[4], and Hyuk-Jae Edward Kwon[1,*]

[1]Department of Oral Biology, School of Dental Medicine, University at Buffalo, The State University of New York, Buffalo, NY 14214, U.S.A.;
[2]Department of Biochemistry, Jacobs School of Medicine and Biomedical Sciences, Institute for Myelin and Glia Exploration, University at Buffalo, The State University of New York, Buffalo, NY 14203, U.S.A.;
[3]Department of Biological Sciences, College of Arts and Sciences, FOXG1 Research Center, University at Buffalo, The State University of New York, Buffalo, NY 14260, U.S.A.;
[4]Department of Systems Pharmacology & Translational Therapeutics, Institute for Immunology, University of Pennsylvania, PA 19104, U.S.A.

*Corresponding authors:

Hyuk-Jae Edward Kwon, D.D.S., Ph.D.
Department of Oral Biology
School of Dental Medicine
University at Buffalo, The State University of New York
547 Biomedical Research Building
Buffalo, NY 14214-8024, U.S.A.
hekwon@buffalo.edu

Jung-Mi Lee, Ph.D.
Department of Oral Biology
School of Dental Medicine
University at Buffalo, The State University of New York
540 Biomedical Research Building
Buffalo, NY 14214-8024, U.S.A.
jungmile@buffalo.edu

Abstract

MLL4, also known as KMT2D, is a histone methyltransferase that acts as an important epigenetic regulator during various organogenesis programs. Mutations in the *MLL4* gene are the major cause for Kabuki syndrome, a human developmental disorder that involves craniofacial birth defects, including anomalies in the palate. The purpose of this study was to investigate the role of Mll4 and the underlying mechanisms in the development and growth of the palate. We generated a novel conditional knockout (cKO) mouse model with tissue-specific deletion of *Mll4* in the palatal mesenchyme. By using micro-computed tomography (CT), histology, cell mechanism assays, and gene expression analysis approaches, we examined the development and growth of the palate in the *Mll4*-cKO mice. Gross intra-oral examination at adult stages showed that *Mll4*-cKO mice had defects along the midline of the palate, which included disrupted rugae pattern and widened midpalatal suture. Micro-CT-based skeletal analysis in the adult mice revealed that the overall palate width was decreased in the *Mll4*-cKO mice. By using whole-mount and histological staining approaches at perinatal stages, we identified that the midline defects started to appear as early as 1 day prior to birth, manifesting initially as a widened midpalatal suture, accompanied by increased cell apoptosis in the suture mesenchyme cells. Genome-wide analysis of mRNA expression in the midpalatal suture tissue showed that Mll4 is essential for timely expression of major genes for cartilage development, such as *Col2a1* and *Acan*, at birth. These results were validated through immunofluorescence staining, confirming that the expression of chondrogenic markers Sox9 and Col2a1 were markedly decreased, whereas that of the osteogenic marker Runx2 remained unchanged, in the midpalatal suture of the *Mll4*-cKO mice. Indeed, time-course histological analysis during postnatal palate growth revealed retardation in the development of the suture cartilage in the *Mll4*-cKO mice. In parallel, time-course micro-CT analysis during postnatal palatogenesis confirmed a transverse growth deficit in the palate of the *Mll4*-cKO mice. Taken together, our results show that Mll4 is essential for timely occurrence of key cellular and molecular events that lead to proper midpalatal suture development and palate growth.

Introduction

The palate is a central structure in the craniofacial complex, playing a crucial role in breathing, feeding, speech, and maintaining overall craniofacial health. Thus, palatogenesis—the development and growth of the palate—is a vital process in establishing the craniofacial complex. Palatogenesis can be broadly divided into two phases: embryonic palatogenesis and postnatal palatogenesis, which occurs very similarly in humans and mice (Dixon et al., 2011). The first phase, embryonic palatogenesis, occurs during the early stages of fetal development and involves the initial formation of a pair of palatal shelves, which are bilateral outgrowths from the left and right maxillary processes, at embryonic day (E) 11 in mice. These bilateral palatal shelves then undergo remodeling, grow toward the midline, and fuse with each other between E12 and E15, establishing the foundational structure of the palate (Bush and Jiang, 2012). The second phase, postnatal palatogenesis, involves bone formation and skeletal growth, which occurs along the anteroposterior and transverse directions, with the palate reaching its full adult dimension by 5 weeks of age in mice. A key feature in postnatal palatogenesis is the role of the midpalatal suture, which remains active postnatally, allowing for the transverse growth of the palate and the accommodation of the growing craniofacial complex during the growth spurts of childhood and adolescence (Griffiths et al., 1967, Latham, 1971). For example, surgical disruption in the developing mouse midpalatal suture may result in narrow palate and midfacial hypoplasia (Li et al., 2015). Both phases are crucial for the functional integrity of the palate, and their regulation is orchestrated by a complex interplay of genetic and epigenetic factors, ensuring the precise expression of developmental genes at the right time and place (Li et al., 2017). Any disruption in these factors may lead to severe birth defects such as orofacial clefts, which are among the most common congenital anomalies (Garland et al., 2020, Reynolds et al., 2020). This direct clinical relevance has driven substantial research efforts to understand embryonic palatogenesis. In contrast, postnatal palatogenesis remains significantly understudied, especially regarding the underlying mechanisms, which has contributed to disparity in research focus. Thus, there is a critical need to expand research into postnatal palatogenesis to address issues related to functional impairments and orthodontic concerns that can arise later in life and to better understand the complete picture of craniofacial development.

Epigenetic regulation, including histone modification, plays a pivotal role in orchestrating craniofacial development and growth (Shull and Artinger, 2024). By regulating chromatin structure and accessibility, epigenetic regulation ensures precise temporal and spatial expression of genes essential for establishing the craniofacial structures in health and disease, influencing cellular mechanisms, such as proliferation, migration, and differentiation. In this regard, mixed lineage leukemia 4 (MLL4), also known as histone-lysine *N*-methyltransferase 2D (KMT2D), is a plausible candidate that may serve as a key epigenetic regulator in palatogenesis. MLL4 is a histone H3 lysine 4 (H3K4) methyltransferase that plays a crucial role in modulating gene expression patterns that are fundamental to the establishment and maintenance of cell identity and lineage specificity during organogenesis (Froimchuk et al., 2017). Mutations in *MLL4* cause Kabuki syndrome, which is a human developmental disorder characterized by distinctive facial features including eversion of lower lateral eyelids and elongated palpebral fissures, postnatal growth retardation, intellectual disability, and skeletal, craniofacial, and dermatoglyphic abnormalities (Boniel et al., 2021). Within the craniofacial complex, Kabuki syndrome is associated with orofacial anomalies, including various palate anomalies and midfacial dysplasia (Matsune et al., 2001). Previous studies using various animal models have shown that *Mll4* plays an important role in craniofacial development by regulating neural crest formation, migration, and differentiation (Bögershausen et al., 2015, Schwenty-Lara et al., 2020, Van Laarhoven et al., 2015). Notably, mice with tissue-specific deletion of *Mll4* in the neural crest cell-lineage, driven by either *Wnt1-Cre* or *Sox10-Cre*, showed cleft palate (Shpargel et al., 2020). This suggests that palatal shelf fusion during embryonic palatogenesis requires *Mll4* function in the cranial neural crest-derived cells, which give rise to the palate mesenchyme. However, deletion of *Mll4* in these mice occurs considerably earlier than the initiation of palatogenesis (at E11). Therefore, it remains uncertain whether the cleft palate phenotype is a result of *Mll4* deficiency during or prior to the initiation of palatogenesis. Moreover, due to the neonatal lethality, these neural crest-specific *Mll4* deletion mice were limited to investigating only the embryonic palatogenesis. Thus, there is a critical need to understand the comprehensive role and underlying mechanism of Mll4 in palatogenesis in a time- and tissue-specific manner.

In this study, we aimed to elucidate the comprehensive role and the underlying mechanism by which Mll4 regulates palatogenesis. We first generated a novel mouse model with palatogenesis-specific *Mll4* deletion (*Mll4*$^{fl/fl}$*;Osr2-Cre*) and used micro-computed tomography (CT), histology, cell mechanism assays, and

gene expression analysis approaches to examine the development and growth of the palate in our mouse model. We revealed that *Mll4* deficiency results in retardation in the developmental of the midpalatal suture and transverse growth deficits during postnatal palatogenesis. Our study provides insight into the intrinsic role of Mll4 in palatogenesis, which informs the physiological developmental mechanism and therapeutic strategies for congenital orofacial anomalies.

Materials and Methods

Mouse Strains

Osr2-Cre (originally described as '*Osr2KI*-Cre') (Chen et al., 2009, Shpargel et al., 2020), and *Mll4*$^{fl/fl}$ (Lee et al., 2013) lines were used for generating an *Mll4* conditional knockout (cKO) model. *ROSA*$^{mT/mG}$ (hereafter referred to as *mTmG*) reporter line (Muzumdar et al., 2007) was used to label palate mesenchyme cells expressing eGFP by crossing with *Osr2-Cre* line. Mice were maintained by intercrossing or by crossing with C57BL/6J inbred mice. All animal procedures were approved by the Institutional Animal Care and Use Committee at the University at Buffalo.

Micro-CT Scanning and 3-Dimensional Reconstruction

The heads of mice aged 1, 3, 6, and 10 weeks were fixed in 10% formalin overnight and subsequently washed with PBS. Micro-CT scans were performed using a SCANCO µCT 100 (SCANCO Medical, Switzerland) (voxel size, 10 µm). The scanned images were calibrated to milligrams of hydroxyapatite per cubic centimeter (mgHA/cm^3) for accurate density measurement. Each image was manually adjusted for rotation and alignment along each axis using the FIJI software (Schindelin et al., 2012). To eliminate background noise, areas with measurements below 200.03 mgHA/cm^3 were removed. Each image was then cropped to focus on the specific region of interest within the maxillary jaw. The Fijiyama plugin was used to manually register the images, aligning them for further analysis (Fernandez and Moisy, 2021). Finally, the 3Dscript plugin was used for 3-dimensional (3D) rendering (Schmid et al., 2019).

Histology and Immunofluorescence Staining

Mice were euthanized at predetermined stages. Head tissue specimens were fixed in 4% paraformaldehyde (PFA), dehydrated through an ethanol series, embedded in paraffin, and sectioned at 5–7 µm thickness, as described previously (Lee et al., 2022). Specimens harvested at E18.5, and postnatal 1, 3, 6, and 10 weeks were decalcified in 14% ethylenediaminetetraacetic acid (EDTA) for 1, 3, 6, and 10 weeks, respectively. For histological analysis, sections were stained with Azan's trichrome staining, as previously described (Lee et al., 2022), and were imaged on an Axioscope compound upright light microscope (for 20X and 40X magnifications)

(Zeiss, Germany). An SZX16 stereomicroscope (Olympus, Japan) was used for 5X magnification images, as well as gross images. For immunofluorescence staining, antigen retrieval was performed in an antigen retrieval buffer, using a pressure cooker for 15 min at low pressure, followed by washing in PBS, blocking at room temperature in a blocking buffer (2% goat serum, 5% BSA, 1% Triton-X 100, 0.1% Tween-20 in PBS) for 1 hr, and incubation with primary antibodies, diluted in blocking buffer, overnight at 4°C. On the second day, the sections were washed in PBS, incubated with secondary antibodies, diluted in blocking buffer, at room temperature for 1 hr, washed in PBS, and mounted with Vectashield mounting media with DAPI (Vector Laboratories, USA; H-1200). The primary antibodies used were: homemade guinea pig anti-Mll4 (1:300) (Huisman et al., 2021), rabbit monoclonal anti-Sox9 (1:300; Abcam, UK; ab185230), mouse monoclonal anti-Col2a1 (1:50, Santa Cruz, USA; sc-52658), and rabbit monoclonal anti-Runx2 (1:300; Cell Signaling, USA; #12556). Immunofluorescence images were acquired using a THUNDER Imager fluorescence microscope (Leica Microsystems, USA).

TUNEL Assay

The DeadEnd™ Fluorometric TUNEL System (Promega, USA; G3250) was used to assess apoptosis in paraffin sections, according to the manufacturer's protocol.

Skeletal Preparations

Mouse heads, harvested at predetermined stages, were fixed in 100% ethanol for 3 days, stained in Alcian Blue solution (30 mg Alcian Blue dissolved in 20 ml glacial acetic acid plus 80 ml 95% ethanol) for 2 days, re-fixed in 100% ethanol for 24 hr, cleared in 2% KOH for 3 hr, and counterstained in Alizarin Red solution (50 mg Alizarin Red dissolved in 1 L of 1% KOH) for 24 hr, followed by tissue clearing in 1% KOH/20% glycerol for 3 days. Images were acquired using a standard stereomicroscope (Amscope, USA).

RNA-Seq and Bioinformatics Analysis

Total RNA was extracted from micro-dissected midpalatal suture tissue samples using the RNeasy Micro Plus Kit (Qiagen, Germany; 74034). 4 biological replicates per each genotype, control and *Mll4*-cKO, were used for sequencing (1 sample in each genotype was pooled from 3 individuals). Library construction and high-

throughput sequencing (Illumina NovaSeq PE150) were performed by Novogene company (China). Sequencing reads were analyzed using Salmon (Patro et al., 2017) to quantify gene expression at the transcript level. These Salmon outputs were analyzed using DESeq2 (Love et al., 2014) to obtain gene expression information at the gene level and identify differentially expressed genes (DEGs) between *Mll4*-cKO and littermate control samples. DEGs were defined by a log2 fold change (log2FC) ≥ 0.4 and an adjusted p-value ≤ 0.001. Volcano plots were generated using the EnhancedVolcano package (Blighe et al., 2024). Gene ontology analysis was performed using clusterProfiler (Wu et al., 2021). The original RNA-seq data files will be deposited into the National Center for Biotechnology Information Gene Expression Omnibus (NCBI GEO) database.

Statistics

All statistical analyses were performed using Prism 10 software (GraphPad Software, USA). Pairwise differential expression was analyzed using Student's t-test. Statistical significance was defined as p-values ≤ 0.05 (*), ≤ 0.01 (**), and ≤ 0.001 (***).

Results

Generating a novel *Mll4* deficiency model for studying the palate tissue-autonomous role of Mll4 during palate development and growth

For the purpose of investigating the role of Mll4 specifically during palatogenesis, we used the Cre/loxP system driven by *Osr2-Cre*. *Osr2-Cre* is first activated at E11, when palatogenesis is initiated, and remains active in the palate mesenchyme cells (Lan et al., 2001, Lan et al., 2004). By using the *Osr2-Cre;mTmG* mice, we can confirm the activation of *Osr2-Cre* by using fluorescence microscopy and detecting GFP signals. When the bilateral palatal shelves are actively undergoing morphogenesis, for example at E13.5, *Osr2-Cre* was activated in the developing palatal shelves, which occupies the center of the developing face (Fig. 1A, B). Thus, we were able to generate a novel mouse model with palatogenesis-specific deletion of *Mll4* in the palate mesenchyme cells (*Mll4*$^{fl/fl}$*;Osr2-Cre*, or *Mll4*-cKO). Surprisingly, compared to the previously reported neural crest-specific *Mll4* deletion (*Mll4*$^{fl/fl}$*;Wnt1-Cre* and *Mll4*$^{fl/fl}$*;Sox10-Cre*) mice, which exhibited cleft palate and neonatal lethality (Shpargel et al., 2020), our palatogenesis-specific *Mll4*-cKO mice did not show cleft palate or lethality at birth and could grow up into adult mice that did not show much noticeable changes when grossly examined for exterior appearance at 10 weeks (Fig. 1C, D, F, G). However, by closely examining the intra-oral aspect of the palate, we discovered several minor differences between the control and *Mll4*-cKO mice (Fig. 1E, H). Compared to controls, *Mll4*-cKO mice showed altered rugae pattern—especially, ruga number 3 was discontinuous in the midline (Fig. 1E′, H′, arrows). Also, the midpalatal suture was more widened in the *Mll4*-cKO palate, compared to the control palate (Fig. 1E′, H′, arrowheads). To test the possibility that this palate phenotype that we observed in the *Mll4*-cKO mice may have resulted from delay in their overall development and growth, we measured the body weight both at 10 weeks and at birth but did not find any significant difference (Fig. 1I). We also compared the body weight between male and female mice at these two stages but found no significant difference (data not shown). Our initial observations suggested that, separate from its early role in neural crest cell differentiation, Mll4 may have other unknown functions in postnatal palate development and growth.

Thus, to gain better understanding of the palate phenotype observed from gross intra-oral examination of the *Mll4*-cKO mice (Fig. 1), we further examined the palate skeleton at 10 weeks by using micro-CT

analysis. By examining the virtual 3D models that were created by reconstructing the planar X-ray images, we found that the overall palate width showed narrowing in the *Mll4*-cKO mice. Anatomical landmarks for assessing the palate width, such as the incisive foramens, palatal processes of maxilla, and palatal processes of palatine, all showed constricted appearances in the virtual 3D model of the *Mll4*-cKO mice (Fig. 2A, B). Using virtual slicing of the 3D models, we were able to further generate digital coronal/frontal cross sections of the palate. These virtual cross sections enabled us to perform quantitative analysis of the horizontal dimension of the palate along its anteroposterior axis. Thus, using this method, we examined the overall width of the palate by precisely measuring the width of the incisive foramens (in slice 1), the palatal processes of maxilla (in slice 2), the transpalatal suture (in slice 3), and the palatal processes of palatine (in slice 4) at the four representative section levels (Fig. 2C, D). At all four section levels along the anteroposterior axis, the palate width showed significant decrease in the *Mll4*-cKO mice, compared to the control mice (Fig. 2E). These results suggested that Mll4 plays an important role in transverse growth of the palate during postnatal palatogenesis.

Mll4 deficiency results in initial formation of a wider midpalatal suture with increased cell apoptosis at birth

We next asked the question of how Mll4 promotes palate growth. Based on our finding that the adult *Mll4*-cKO mice showed significant narrowing of the palate at 10 weeks (Fig. 2), we reasoned that the key biological events for palate growth that depend on *Mll4* function may occur at younger ages, possibly as early as, or even prior to, birth. Thus, to identify the primary developmental mechanism underlying the role of Mll4 in palate growth, we examined the palate anatomy in the control and *Mll4*-cKO mice around birth, searching for the earliest signs of disruption in the *Mll4*-cKO palate. By first using skeletal staining of the developing cranium and palate tissues, we found that the overall skeletal pattern was similar between the control and *Mll4*-cKO mice (Fig. 3A, B). However, when carefully inspecting the midline, where we had initially observed discontinuous rugae pattern and a more obvious midpalatal suture in the *Mll4*-cKO mice (Fig. 1), we found that the width of the midpalatal suture was slightly wider in the *Mll4*-cKO mice, compared to the control mice, prior to birth (at E18.5) (Fig. 3A, B, arrowheads). In parallel, histological examination of the palate, by using trichrome staining of the coronal/frontal paraffin sections, confirmed that the width of the midpalatal suture, situated between the bilateral bony palatal processes, were increased in the *Mll4*-cKO mice, compared to the control mice (Fig. 3C,

D, C′, D′). To determine the cellular mechanisms underlying the wider midpalatal suture in the *Mll4*-cKO mice, we performed both cell proliferation, using EdU incorporation, and cell apoptosis, using TUNEL staining, assays. While rarely any cells in the midpalatal suture were EdU-positive for cell proliferation in both the control and *Mll4*-cKO mice (data not shown), TUNEL-positive cell apoptosis showed significant increase in the *Mll4*-cKO, compared to control, midpalatal suture at E18.5 (Fig. 3E–G, E′, F′). Our findings that the earliest signs of disrupted biological events were specifically discovered in the midpalatal suture of the perinatal *Mll4*-cKO palate suggested that Mll4 is essential for the establishment of the midpalatal suture around birth.

Mll4 deficiency results in dysregulation of the timely expression of chondrogenic genes at birth

To gain insight into the molecular mechanism underlying the histological and cellular alterations that we observed in the perinatal *Mll4*-cKO palate tissue, we micro-dissected the midpalatal suture tissues and performed genome-wide mRNA expression analysis (RNA-seq) in the control and *Mll4*-cKO mice at birth (P0.5). Our results showed that a total of 117 genes were differentially expressed between the control and *Mll4*-cKO midpalatal suture tissues, of which 40 genes were upregulated and 77 genes were downregulated in the *Mll4*-cKO group (p-value < 0.001, log2FC > 0.4) (Fig. 4A). Notably among the DEGs were genes associated with cartilage development, or chondrogenesis, which included extracellular matrix genes *Col2a1*, *Col9a1*, *Col9a2*, *Acan* (*Aggrecan*), and *Comp* (*Cartilage oligomeric matrix protein*), as well as *Mia*/*Cdrap1* (*Melanoma inhibitory activity*) and *Snorc* (*Small novel rich in cartilage*). By performing gene ontology (GO) analysis, we identified the top 10-enriched biological processes and generated a list of downregulated genes associated with each of the top 10 biological processes (Fig. 4B–D). Our analysis inferred that cartilage development, endochondral bone morphogenesis, and chondrocyte differentiation were some of the highly enriched biological processes possibly regulated by Mll4. From the list of DEGs identified from our GO analysis (Fig. 4), we selected several representative genes for cartilage and bone development, including *Col2a1*, *Runx2*, and *Sox9*, that were from the highly enriched biological processes and were representative markers for differentiation of the osteochondral progenitor cells during both chondrogenesis and endochondral ossification. We used these markers in order to verify our RNA-seq results by performing immunofluorescence staining in the paraffin sections of the perinatal palate (at P0.5) in control and *Mll4*-cKO mice. In parallel, we also verified with immunofluorescence staining the expression of Mll4 in the perinatal *Mll4*-cKO palate. Our results showed

that the intensity of Col2a1 and Sox9, which both are early chondroblast differentiation markers, were markedly reduced in the *Mll4*-cKO midpalatal suture (Fig. 5B1, D2), compared to controls (Fig. 5A1, C2). In contrast, the intensity of Runx2, which is an osteogenic differentiation marker, showed similar levels in the control and *Mll4*-cKO midpalatal suture (Fig. 5A2, B2). These results suggested that the main molecular events dependent on *Mll4* function in the perinatal midpalatal suture were associated with chondrogenic cell differentiation and cartilage development, and also possibly endochondral ossification. In addition, the markedly reduced intensity of Mll4 in the perinatal *Mll4*-cKO palate indicated that the *Mll4* gene was effectively deleted in the *Mll4*-cKO palate (Fig. 5C1, D1).

Mll4 deficiency leads to retardation of the development of the midpalatal suture

To verify whether the biological processes that were identified from our RNA-seq analysis were actually impacted as a result of *Mll4* deficiency during postnatal palatogenesis, we performed histological examination of the midpalatal suture at birth and beyond (up to 1 week), using trichrome staining of the paraffin sections (Fig. 6). Interestingly, after birth (at P0.75) in the control mice, a newly formed layer of cartilage tissue was capping the medial surface of each of the bilateral palatal processes, flanking the midpalatal suture (Fig. 6A, arrowheads). In contrast, the newborn *Mll4*-cKO mice did not form such midpalatal suture-flanking cartilage tissue layers on the medial surfaces of the bilateral palatal processes (Fig. 6B). By histologically monitoring the postnatal development of the midpalatal suture, we found that, at 1 week in the control mice, the midpalatal suture cartilage layers showed uniform enlargement of the consisting chondrocytes (Fig. 6C, arrowheads). In contrast, the 1-week old *Mll4*-cKO mice just started to develop the midpalatal suture cartilage layers, which were only partially formed (Fig. 6D, arrowheads). Our findings suggested that this defective phenotype observed in the *Mll4*-cKO midpalatal suture cartilage was due to significant retardation of chondrogenic differentiation as a result of *Mll4* deficiency in the developing palate. Thus, we further performed additional time-course examination of the midpalatal suture development at 3, 6, and 10 weeks. Interestingly, at all three stages (3, 6, and 10 weeks), the bilateral cartilage layers in both the control and *Mll4*-cKO midpalatal sutures were shown to be adhered to each other in the midline (Fig. 6E–J). However, the interface between the bilateral cartilage layers was less straight in the *Mll4*-cKO suture, compared to the control suture (Fig. 6E–J). Also at all three stages, the overall width of the midpalatal suture cartilage was markedly increased in the *Mll4*-

cKO mice (brackets in Fig. 6F, H, J) than in the control mice (brackets in Fig. 6E, G, I). In addition, compared to the horizontally organized chondrocyte 'columns' in the control group, the *Mll4*-cKO suture chondrocytes appeared disorganized and were under-differentiated, especially at 10 weeks (Fig. 6I, J, I′, J′). Taken together, these results suggested that *Mll4* deficiency results in retardation in the developmental of the midpalatal suture during postnatal palatogenesis.

Mll4 deficiency leads to deficits in the transverse growth of the palate

In parallel to the time-course histological examination of the midpalatal suture cartilage, we also conducted time-course micro-CT analysis of the palate skeleton at the same time points during postnatal palatogenesis (at 1, 3, 6, and 10 weeks). The main purpose of this approach was to address the question of whether *Mll4* is actually required for proper growth of the palate during postnatal palatogenesis. We also reasoned that it is worth closely monitoring the association between the transverse growth of the palate and the midpalatal suture development, based on the disrupted gene expression (at birth) and the developmental retardation phenotype in the *Mll4*-cKO midpalatal suture during postnatal palatogenesis (at 1, 3, 6, and 10 weeks). Therefore, we conducted a quantitative analysis of the horizontal dimension of the palate skeleton in the micro-CT-generated virtual coronal/frontal cross sections. For this approach, we used the same four representative coronal/frontal cross section levels along the anteroposterior axis of the palate, which we used for our initial skeletal examination at 10 weeks (Fig. 2). At 1 week, we found that palate growth was not significantly changed in the *Mll4*-cKO mice at the incisive foramen level (Fig. 7A). In contrast, at the rest of the levels, the first (M1), second (M2), and third molar (M3) levels, palate growth showed minor, but significant decrease (Fig. 7B–D). Later, at 3, 6, and 10 weeks, palate growth showed significant decrease at all four levels along the anteroposterior axis in the *Mll4*-cKO mice, compared to the control mice (Fig. 7A–D). These results suggested that *Mll4* is indeed required for proper transverse growth of the palate during postnatal palatogenesis. By integrating our findings in the developing midpalatal suture and in the growing palate skeleton, our data suggest that *Mll4* is associated with midpalatal suture development and palate growth during postnatal palatogenesis.

Discussion

A newly developed *Mll4* deficiency/Kabuki syndrome mouse identifies a novel role of Mll4 in determining palate width during postnatal palatogenesis

In this study, we generated for the first time a unique mouse model that shows that Mll4 is essential for determining the width of the palate. Driven by *Osr2-Cre*, *Mll4* was deleted tissue-specifically in the palate mesenchyme, starting at the onset of palatogenesis (at E11) (Lan et al., 2001, Lan et al., 2004), allowing us to examine the intrinsic role of *Mll4* specifically during the actual palatogenesis process. These examinations were performed at timepoints that were not limited to the prenatal stages because the *Mll4*-cKO mice did not show cleft palate or neonatal lethality, in contrast to other recently reported neural crest-specific *Mll4* deletion models driven by *Wnt1-Cre* or *Sox10-Cre*, which exhibited cleft palate and neonatal lethality (Shpargel et al., 2020). Importantly, the narrow palate phenotype, in fact, closely resembles a common craniofacial phenotype for Kabuki syndrome, the high-arched and narrow palate, which was reported to be found in 72% (64 out of 89) of individuals with Kabuki syndrome (Matsumoto and Niikawa, 2003, Porntaveetus et al., 2018). This frequency was twice as high as the 35% (68/196) frequency in Kabuki syndrome for the cleft lip/palate phenotype (Matsumoto and Niikawa, 2003), which was mainly studied using the aforementioned neural crest-specific *Mll4* deletion mice (Shpargel et al., 2020). Moreover, the narrow palate phenotype shown in our *Mll4*-cKO model is of high clinical relevance because of its potential risk in human conditions of causing various dental and orofacial problems, such as crowded or impacted teeth, breathing difficulty, and midfacial hypoplasia. Our unique *Mll4*-cKO model enabled us to address not only a particularly significant craniofacial problem in Kabuki syndrome but also a critical developmental process that has been understudied but requires urgent attention. This informs the multifaceted role of Mll4 in craniofacial development and disease.

Mll4 is essential for proper development of the midpalatal suture

Here, we demonstrated the sequential development of the bilateral secondary cartilage layers in the midpalatal suture of wildtype mice, from prenatal to adult stages. In comparison, we showed that, in the absence of *Mll4*, the initial appearance of these cartilage tissues was significantly delayed, and the midpalatal suture continued to exhibit developmental deficits as the mice grew older. By performing whole gene expression profiling in the

midpalatal suture tissues, we identified that *Mll4* is required for the timely expression of a large number of genes related to chondrogenesis. Interestingly, these chondrogenic genes, including *Col2a1* (Bell et al., 1997, Lefebvre et al., 1997, Ng et al., 1997), *Col9a1* (Genzer and Bridgewater, 2007, Zhang et al., 2003, Zhou et al., 1998), *Col9a2* (Bernard et al., 2003), *Acan* (Sekiya et al., 2000, Han and Lefebvre, 2008), *Comp* (Liu et al., 2007), *Mia*/*Cdrap1* (Xie et al., 1999), and *Snorc* (Jaiswal et al., 2020), were all shown to be commonly activated by the Sox9 transcription factor, a known master regulator for chondrogenesis (Lefebvre et al., 2019). Our immunofluorescence results, in addition, showed that Sox9 expression was markedly downregulated specifically in the mesenchyme cells in the *Mll4*-cKO midpalatal suture. Notably, SOX9 was recently identified to act as a pioneer factor that recruits epigenetic co-factors, including Mll4, in order to epigenetically prime and remodel the chromatin to a transcriptionally accessible state during cell fate determination (Yang et al., 2023). Therefore, it is reasonable to speculate that *Mll4* deficiency may have a dual impact on the development of the midpalatal suture in the *Mll4*-cKO mice: firstly, due to the unavailability of Mll4, as a transcriptional co-activator of Sox9, in creating a transcriptionally active chromatin landscape; secondly, due to the downregulated expression of Sox9 itself. Both scenarios would lead to an impairment of Sox9's ability to effectively activate the expression of its downstream chondrogenic genes, as shown in the *Mll4*-cKO midpalatal suture. Furthermore, Sox9 is known for its auto-regulatory function in chondrocytes (Mead et al., 2013), which might exacerbate the Sox9-driven chondrogenesis defects in our model. Additionally, Sox9 is known to regulate apoptosis in the neural crest cells (Cheung et al., 2005), suggesting that Sox9 deficiency may also account for the increased number of TUNEL-positive apoptotic cells in the *Mll4*-cKO midpalatal suture (Fig. 3E–G).

The chondrogenic retardation in our model is in agreement with previously reported chondrogenic defect phenotypes in the cartilaginous primordia of the cranial base in the neural crest-specific *Mll4* deletion mice, as well as in the growth plate of the long bones in the heterozygous *Mll4* loss-of-function mice (Fahrner et al., 2019, Shpargel et al., 2020). By comparing our DEG list with another DEG list from an RNA-seq dataset in earlier palatal shelves (at E14.25) of the neural crest-specific *Mll4* deletion mice (Shpargel et al., 2020), we found that a subpopulation of our identified *Mll4*-downstream chondrogenic genes, *Acan*, *Col2a1*, *Col9a1*, *Col9a2*, *Col9a3*, and *Mia*, were commonly down-regulated in both studies. These findings provide insight into a possible consensus regulatory mechanism downstream of Mll4 in different states of cell differentiation at

different stages of palatogenesis. Among these commonly down-regulated genes, *Acan* and *Col2a1* were identified as cleft palate causal genes (Xu et al., 2021), which suggests a common mechanism underlying the etiology of two different phenotypes: narrow palate and cleft palate, which may manifest differently depending on distinct molecular contexts at the time of their onset. These possibilities are supported by research indicating that high-arched and narrow palate and cleft palate can share common genetic causes (Conley et al., 2016, Tabler et al., 2013), which would be interesting to further verify in the future. On the other hand, these commonly down-regulated genes also raise the question of why the developing bilateral palatal shelves fail to fuse only in the neural crest-specific *Mll4* deletion mice, resulting in cleft palate, but not in our palate mesenchyme-specific *Mll4*-cKO mice. This may be explained by the possibility that *Mll4* is required for palatal shelf fusion prior to palatogenesis, possibly during the stage when migratory neural crest cells have not yet differentiated into palate mesenchyme cells. Therefore, the cleft palate phenotype observed in the neural crest-specific *Mll4* deletion mice may be due to a secondary effect resulting from an earlier developmental deficit.

Mll4 regulates midpalatal suture development, mediating palate growth during postnatal palatogenesis

The midpalatal suture has long been regarded as a critical skeletal structure that is anatomically situated in the very center of the craniofacial complex, playing a significant role in the development and growth of the palate and the maxillary jaw (Latham, 1971, Li et al., 2015, Rice, 2008). Therefore, it is intriguing to discover that the two major phenotypes observed in the *Mll4*-cKO mice were the growth deficit in the palate and the developmental retardation of the midpalatal suture. These two findings, in the midpalatal suture and in the overall palate width, support our proposed model, emphasizing the central role of Mll4 in driving transverse palate growth and establishing the physiologically normal dimension of the palate by regulating the development of the midpalatal suture. Our study provides insight into the epigenetic mechanisms in palatogenesis regulated by Mll4, which could enhance our understanding of palatogenesis and advance therapeutic strategies for craniofacial disorders.

An important feature of the midpalatal suture, that is of high clinical relevance, is that it not only functions as a growth site that drives postnatal palate growth but also, in reverse, biologically responds to mechanical forces exerted from its environment, for example, due to growth of the palatal and maxillary skeleton or suckling and masticatory oral movements (Roth et al., 2022, Li et al., 2016). In orthodontic

dentistry, as another example, the rapid palatal expansion procedure uses a device that exerts mechanical force to the maxillary jaw, causing widening of the midpalatal suture, leading to tensile force, inducing new bone formation in the midpalatal suture, and effectively increasing the width of the maxillary jaw. These biological responses to tensile force may be explained, at least partially, by a chondrogenic mesenchyme cell subpopulation in the midpalatal suture that expresses *Piezo2*, an ion channel gene associated with mechanosensation, which was recently identified in a single cell transcriptomics study (Gao et al., 2022). Therefore, it would be interesting to test whether *Mll4* deficiency impacts the response to mechanical cues in the *Piezo2*-positive chondrogenic mesenchyme cells in the midpalatal suture, which can be simulated by performing the palatal expansion procedure on the *Mll4*-cKO mice (Hou et al., 2007, Katebi et al., 2012).

Data Availability Statement
RNA-seq data will be deposited in the NCBI GEO database.

Ethics Statement
The animal study was reviewed and approved by Institutional Animal Care and Use Committee (IACUC) at the University at Buffalo.

Author Contributions
J-ML acquired funding, conceptualized, designed, administered, and supervised the research, performed experiments, acquired data, conducted data analysis and visualization, wrote and edited the manuscript. HJ performed experiments, acquired data, conducted data analysis and visualization, and edited the manuscript. BdPMP performed experiments, acquired data, conducted data analysis and visualization, and edited the manuscript. YP conducted data analysis and visualization and edited the manuscript. SJ provided resources. S-KL acquired funding for the project, provided resources, and edited the manuscript. JWL acquired funding for the project, provided resources, and edited the manuscript. H-JEK acquired funding, conceptualized, designed, administered, and supervised the research, performed experiments, acquired data, conducted data analysis and visualization, wrote and edited the manuscript. All authors contributed to and approved the publication of the manuscript.

Funding
This study was supported by the National Institutes of Health's (NIH's) National Center for Advancing Translational Sciences (KL2TR001413 and UL1TR001412 to H-JEK) and National Institute of Dental and Craniofacial Research (T32DE023526 to J-ML; R03DE030985 to H-JEK).

Conflict of Interest
All authors declare that the research was conducted in the absence of any commercial or financial relationships that could be construed as a potential conflict of interest.

Acknowledgements
We thank Andrew D. McCall at the Optical Imaging and Analysis Facility (OIAF), School of Dental Medicine, The State University of New York at Buffalo, for assistance in acquiring micro-CT data and gross, histology, and stereo immunofluorescence images, which were all conducted at the OIAF. We thank Yang Chai at the University of Southern California for providing the *Osr2-Cre* mouse strain. We thank Eun-Myung Mary Song and Monique M. Kapur-Mauleon for assistance with experiments. We would also like to thank the members of the Kwon lab for their helpful comments and feedback.

References

BELL, D. M., LEUNG, K. K., WHEATLEY, S. C., NG, L. J., ZHOU, S., LING, K. W., SHAM, M. H., KOOPMAN, P., TAM, P. P. & CHEAH, K. S. 1997. SOX9 directly regulates the type-II collagen gene. *Nat Genet,* 16**,** 174-8.

BERNARD, P., TANG, P., LIU, S., DEWING, P., HARLEY, V. R. & VILAIN, E. 2003. Dimerization of SOX9 is required for chondrogenesis, but not for sex determination. *Human Molecular Genetics,* 12**,** 1755-1765.

BLIGHE, K., S, R. & M, L. 2024. *EnhancedVolcano: Publication-ready volcano plots with enhanced colouring and labeling* [Online]. Available: https://github.com/kevinblighe/EnhancedVolcano [Accessed].

BÖGERSHAUSEN, N., TSAI, I. C., POHL, E., KIPER, P., BELEGGIA, F., PERCIN, E. F., KEUPP, K., MATCHAN, A., MILZ, E., ALANAY, Y., KAYSERILI, H., LIU, Y., BANKA, S., KRANZ, A., ZENKER, M., WIECZOREK, D., ELCIOGLU, N., PRONTERA, P., LYONNET, S., MEITINGER, T., STEWART, A. F., DONNAI, D., STROM, T. M., BODUROGLU, K., YIGIT, G., LI, Y., KATSANIS, N. & WOLLNIK, B. 2015. RAP1-mediated MEK/ERK pathway defects in Kabuki syndrome. *J Clin Invest,* 125**,** 3585-99.

BONIEL, S., SZYMAŃSKA, K., ŚMIGIEL, R. & SZCZAŁUBA, K. 2021. Kabuki Syndrome-Clinical Review with Molecular Aspects. *Genes (Basel),* 12.

BUSH, J. O. & JIANG, R. 2012. Palatogenesis: morphogenetic and molecular mechanisms of secondary palate development. *Development,* 139**,** 231-43.

CHEN, J. Q., LAN, Y., BAEK, J. A., GAO, Y. & JIANG, R. L. 2009. Wnt/beta-catenin signaling plays an essential role in activation of odontogenic mesenchyme during early tooth development. *Developmental Biology,* 334**,** 174-185.

CHEUNG, M., CHABOISSIER, M. C., MYNETT, A., HIRST, E., SCHEDL, A. & BRISCOE, J. 2005. The transcriptional control of trunk neural crest induction, survival, and delamination. *Dev Cell,* 8**,** 179-92.

CONLEY, Z. R., HAGUE, M., KUROSAKA, H., DIXON, J., DIXON, M. J. & TRAINOR, P. A. 2016. A quantitative method for defining high-arched palate using the mutant mouse as a model. *Developmental Biology,* 415**,** 296-305.

DIXON, M. J., MARAZITA, M. L., BEATY, T. H. & MURRAY, J. C. 2011. Cleft lip and palate: understanding genetic and environmental influences. *Nat Rev Genet,* 12**,** 167-78.

FAHRNER, J. A., LIN, W. Y., RIDDLE, R. C., BOUKAS, L., DELEON, V. B., CHOPRA, S., LAD, S. E., LUPERCHIO, T. R., HANSEN, K. D. & BJORNSSON, H. T. 2019. Precocious chondrocyte differentiation disrupts skeletal growth in Kabuki syndrome mice. *JCI Insight,* 4.

FERNANDEZ, R. & MOISY, C. 2021. Fijiyama: a registration tool for 3D multimodal time-lapse imaging. *Bioinformatics,* 37**,** 1482-1484.

FROIMCHUK, E., JANG, Y. & GE, K. 2017. Histone H3 lysine 4 methyltransferase KMT2D. *Gene,* 627**,** 337-342.

GAO, L., XU, T., ZHANG, L., LI, Y., YAN, T., YU, G. & CHEN, F. 2022. Midpalatal Suture: Single-Cell RNA-Seq Reveals Intramembrane Ossification and Piezo2 Chondrogenic Mesenchymal Cell Involvement. *Cells,* 11.

GARLAND, M. A., REYNOLDS, K. & ZHOU, C. J. 2020. Environmental mechanisms of orofacial clefts. *Birth Defects Res,* 112**,** 1660-1698.

GENZER, M. A. & BRIDGEWATER, L. C. 2007. A Col9a1 enhancer element activated by two interdependent SOX9 dimers. *Nucleic Acids Res,* 35**,** 1178-86.

GRIFFITHS, D. L., FURSTMAN, L. & BERNICK, S. 1967. Postnatal development of the mouse palate. *Am J Orthod,* 53**,** 757-68.

HAN, Y. & LEFEBVRE, V. 2008. L-Sox5 and Sox6 drive expression of the aggrecan gene in cartilage by securing binding of Sox9 to a far-upstream enhancer. *Mol Cell Biol,* 28**,** 4999-5013.

HOU, B., FUKAI, N. & OLSEN, B. R. 2007. Mechanical force-induced midpalatal suture remodeling in mice. *Bone,* 40**,** 1483-1493.

HUISMAN, C., KIM, Y. A., JEON, S., SHIN, B., CHOI, J., LIM, S. J., YOUN, S. M., PARK, Y., K, C. M., KIM, S., LEE, S. K., LEE, S. & LEE, J. W. 2021. The histone H3-lysine 4-methyltransferase Mll4 regulates the development of growth hormone-releasing hormone-producing neurons in the mouse hypothalamus. *Nat Commun,* 12**,** 256.

JAISWAL, P. K., ALJEBALI, L., GAUMOND, M. H., OH, C. D., YASUDA, H. & MOFFATT, P. 2020. Biochemical characteristics of the chondrocyte-enriched SNORC protein and its transcriptional regulation by SOX9. *Sci Rep,* 10**,** 7790.

KATEBI, N., KOLPAKOVA-HART, E., LIN, C. Y. & OLSEN, B. R. 2012. The mouse palate and its cellular responses to midpalatal suture expansion forces. *Orthod Craniofac Res,* 15**,** 148-58.
LAN, Y., KINGSLEY, P. D., CHO, E. S. & JIANG, R. L. 2001. Osr2, a new mouse gene related to Drosophila odd-skipped, exhibits dynamic expression patterns during craniofacial, limb, and kidney development. *Mechanisms of Development,* 107**,** 175-179.
LAN, Y., OVITT, C. E., CHO, E. S., MALTBY, K. M., WANG, Q. R. & JIANG, R. L. 2004. Odd-skipped related 2 (Osr2) encodes a key intrinsic regulator of secondary palate growth and morphogenesis. *Development,* 131**,** 3207-3216.
LATHAM, R. A. 1971. The development, structure and growth pattern of the human mid-palatal suture. *J Anat,* 108**,** 31-41.
LEE, J. E., WANG, C., XU, S., CHO, Y. W., WANG, L., FENG, X., BALDRIDGE, A., SARTORELLI, V., ZHUANG, L., PENG, W. & GE, K. 2013. H3K4 mono- and di-methyltransferase MLL4 is required for enhancer activation during cell differentiation. *Elife,* 2**,** e01503.
LEE, J. M., QIN, C., CHAI, O. H., LAN, Y., JIANG, R. & KWON, H. E. 2022. MSX1 Drives Tooth Morphogenesis Through Controlling Wnt Signaling Activity. *J Dent Res,* 101**,** 832-839.
LEFEBVRE, V., ANGELOZZI, M. & HASEEB, A. 2019. SOX9 in cartilage development and disease. *Current Opinion in Cell Biology,* 61**,** 39-47.
LEFEBVRE, V., HUANG, W., HARLEY, V. R., GOODFELLOW, P. N. & DE CROMBRUGGHE, B. 1997. SOX9 is a potent activator of the chondrocyte-specific enhancer of the pro alpha1(II) collagen gene. *Mol Cell Biol,* 17**,** 2336-46.
LI, C., LAN, Y. & JIANG, R. 2017. Molecular and Cellular Mechanisms of Palate Development. *J Dent Res,* 96**,** 1184-1191.
LI, J., JOHNSON, C. A., SMITH, A. A., HUNTER, D. J., SINGH, G., BRUNSKI, J. B. & HELMS, J. A. 2016. Linking suckling biomechanics to the development of the palate. *Sci Rep,* 6**,** 20419.
LI, J. T., JOHNSON, C. A., SMITH, A. A., SALMON, B., SHI, B., BRUNSKI, J. & HELMS, J. A. 2015. Disrupting the intrinsic growth potential of a suture contributes to midfacial hypoplasia. *Bone,* 81**,** 186-195.
LIU, C. J., ZHANG, Y., XU, K., PARSONS, D., ALFONSO, D. & DI CESARE, P. E. 2007. Transcriptional activation of cartilage oligomeric matrix protein by Sox9, Sox5, and Sox6 transcription factors and CBP/p300 coactivators. *Front Biosci,* 12**,** 3899-910.
LOVE, M. I., HUBER, W. & ANDERS, S. 2014. Moderated estimation of fold change and dispersion for RNA-seq data with DESeq2. *Genome Biol,* 15**,** 550.
MATSUMOTO, N. & NIIKAWA, N. 2003. Kabuki make-up syndrome: A review. *American Journal of Medical Genetics Part C-Seminars in Medical Genetics,* 117c**,** 57-65.
MATSUNE, K., SHIMIZU, T., TOHMA, T., ASADA, Y., OHASHI, H. & MAEDA, T. 2001. Craniofacial and dental characteristics of Kabuki syndrome. *Am J Med Genet,* 98**,** 185-90.
MEAD, T. J., WANG, Q., BHATTARAM, P., DY, P., AFELIK, S., JENSEN, J. & LEFEBVRE, V. 2013. A far-upstream (-70 kb) enhancer mediates Sox9 auto-regulation in somatic tissues during development and adult regeneration. *Nucleic Acids Res,* 41**,** 4459-69.
MUZUMDAR, M. D., TASIC, B., MIYAMICHI, K., LI, L. & LUO, L. Q. 2007. A global double-fluorescent cre reporter mouse. *Genesis,* 45**,** 593-605.
NG, L. J., WHEATLEY, S., MUSCAT, G. E. O., CONWAYCAMPBELL, J., BOWLES, J., WRIGHT, E., BELL, D. M., TAM, P. P. L., CHEAH, K. S. E. & KOOPMAN, P. 1997. SOX9 binds DNA, activates transcription, and coexpresses with type II collagen during chondrogenesis in the mouse. *Developmental Biology,* 183**,** 108-121.
PATRO, R., DUGGAL, G., LOVE, M. I., IRIZARRY, R. A. & KINGSFORD, C. 2017. Salmon provides fast and bias-aware quantification of transcript expression. *Nat Methods,* 14**,** 417-419.
PORNTAVEETUS, T., ABID, M. F., THEERAPANON, T., SRICHOMTHONG, C., OHAZAMA, A., KAWASAKI, K., KAWASAKI, M., SUPHAPEETIPORN, K., SHARPE, P. T. & SHOTELERSUK, V. 2018. Expanding the Oro-Dental and Mutational Spectra of Kabuki Syndrome and Expression of KMT2D and KDM6A in Human Tooth Germs. *Int J Biol Sci,* 14**,** 381-389.
REYNOLDS, K., ZHANG, S., SUN, B., GARLAND, M. A., JI, Y. & ZHOU, C. J. 2020. Genetics and signaling mechanisms of orofacial clefts. *Birth Defects Res,* 112**,** 1588-1634.
RICE, D. P. 2008. Craniofacial sutures. Development, disease and treatment. Preface. *Front Oral Biol,* 12**,** xi.
ROTH, D. M., SOUTER, K. & GRAF, D. 2022. Craniofacial sutures: Signaling centres integrating mechanosensation, cell signaling, and cell differentiation. *Eur J Cell Biol,* 101**,** 151258.

SCHINDELIN, J., ARGANDA-CARRERAS, I., FRISE, E., KAYNIG, V., LONGAIR, M., PIETZSCH, T., PREIBISCH, S., RUEDEN, C., SAALFELD, S., SCHMID, B., TINEVEZ, J. Y., WHITE, D. J., HARTENSTEIN, V., ELICEIRI, K., TOMANCAK, P. & CARDONA, A. 2012. Fiji: an open-source platform for biological-image analysis. *Nat Methods,* 9**,** 676-82.

SCHMID, B., TRIPAL, P., FRAAß, T., KERSTEN, C., RUDER, B., GRÜNEBOOM, A., HUISKEN, J. & PALMISANO, R. 2019. 3Dscript: animating 3D/4D microscopy data using a natural-language-based syntax. *Nat Methods,* 16**,** 278-280.

SCHWENTY-LARA, J., NEHL, D. & BORCHERS, A. 2020. The histone methyltransferase KMT2D, mutated in Kabuki syndrome patients, is required for neural crest cell formation and migration. *Hum Mol Genet,* 29**,** 305-319.

SEKIYA, I., TSUJI, K., KOOPMAN, P., WATANABE, H., YAMADA, Y., SHINOMIYA, K., NIFUJI, A. & NODA, M. 2000. SOX9 enhances aggrecan gene promoter/enhancer activity and is up-regulated by retinoic acid in a cartilage-derived cell line, TC6. *Journal of Biological Chemistry,* 275**,** 10738-10744.

SHPARGEL, K. B., MANGINI, C. L., XIE, G., GE, K. & MAGNUSON, T. 2020. The KMT2D Kabuki syndrome histone methylase controls neural crest cell differentiation and facial morphology. *Development,* 147.

SHULL, L. C. & ARTINGER, K. B. 2024. Epigenetic regulation of craniofacial development and disease. *Birth Defects Res,* 116**,** e2271.

TABLER, J. M., BARRELL, W. B., SZABO-ROGERS, H. L., HEALY, C., YEUNG, Y., PERDIGUERO, E. G., SCHULZ, C., YANNAKOUDAKIS, B. Z., MESBAHI, A., WLODARCZYK, B., GEISSMANN, F., FINNELL, R. H., WALLINGFORD, J. B. & LIU, K. J. 2013. Mutant Mice Reveal Shared Mechanisms between Ciliopathies and FGF-Related Syndromes. *Developmental Cell,* 25**,** 623-635.

VAN LAARHOVEN, P. M., NEITZEL, L. R., QUINTANA, A. M., GEIGER, E. A., ZACKAI, E. H., CLOUTHIER, D. E., ARTINGER, K. B., MING, J. E. & SHAIKH, T. H. 2015. Kabuki syndrome genes KMT2D and KDM6A: functional analyses demonstrate critical roles in craniofacial, heart and brain development. *Hum Mol Genet,* 24**,** 4443-53.

WU, T., HU, E., XU, S., CHEN, M., GUO, P., DAI, Z., FENG, T., ZHOU, L., TANG, W., ZHAN, L., FU, X., LIU, S., BO, X. & YU, G. 2021. clusterProfiler 4.0: A universal enrichment tool for interpreting omics data. *Innovation (Camb),* 2**,** 100141.

XIE, W. F., ZHANG, X., SAKANO, S., LEFEBVRE, V. & SANDELL, L. J. 1999. Trans-activation of the mouse cartilage-derived retinoic acid-sensitive protein gene by Sox9. *Journal of Bone and Mineral Research,* 14**,** 757-763.

XU, H. D., YAN, F. F., HU, R. F., SUZUKI, A., IWAYA, C., JIA, P. L., IWATA, J. & ZHAO, Z. M. 2021. CleftGeneDB: a resource for annotating genes associated with cleft lip and cleft palate. *Science Bulletin,* 66**,** 2340-2342.

YANG, Y. H., GOMEZ, N., INFARINATO, N., ADAM, R. C., SRIBOUR, M., BAEK, I., LAURIN, M. & FUCHS, E. 2023. The pioneer factor SOX9 competes for epigenetic factors to switch stem cell fates. *Nature Cell Biology,* 25**,** 1185-+.

ZHANG, P., JIMENEZ, S. A. & STOKES, D. G. 2003. Regulation of human COL9A1 gene expression. Activation of the proximal promoter region by SOX9. *J Biol Chem,* 278**,** 117-23.

ZHOU, G., LEFEBVRE, V., ZHANG, Z. P., EBERSPAECHER, H. & DE CROMBRUGGHE, B. 1998. Three high mobility group-like sequences within a 48-base pair enhancer of the gene are required for cartilage-specific expression. *Journal of Biological Chemistry,* 273**,** 14989-14997.

Figure Legends

Figure 1. Generation of a novel *Mll4*-deficient Kabuki syndrome mouse model for palate studies. A conditional *Mll4*-deficiency mouse model (*Mll4*$^{fl/fl}$*;Osr2-Cre*, or *Mll4*-cKO) was generated, using the Cre/loxP system driven by *Osr2-Cre* for studying postnatal palate development. (A, B) Osr2-Cre activation in the developing midface (A) and palate (B), demonstrated in the *Osr2-Cre;mTmG* mouse at E13.5. ps, palatal shelf (in B). (C–H) Orofacial phenotypes in the control (C–E) and *Mll4*-cKO (F–H) adult mice at 10 weeks: (E′, H′) *Mll4*-cKO mice exhibit disrupted rugae pattern (3–6) and midline defects, such as discontinuous ruga (3, arrows) and widened midpalatal suture (arrowheads). (I) Body weight between the control and *Mll4*-cKO mice did not show significant difference in either adult (*n*=4 and 4 for control and cKO, respectively) or newborn mice (*n*=10 and 6 for control and cKO, respectively).

Figure 2. *Mll4*-deficient mice showed decreased horizontal dimension in the palate. (A–D) Skeletal phenotypes were examined, using micro-CT analysis, in control (A, C) and *Mll4*-cKO (B, D) adult mice at 10 weeks. Virtual 3D (A, B) and coronal/frontal sections (C, D) along the anteroposterior axis at four representative levels, at the incisive foramen (slice 1), first molar (slice 2), second molar (slice 3), and third molar (slice 4) levels, were examined. (E) Palate width was measured in each for the four sections that represent the incisive foramen (if) (slice 1), the palatine process of maxilla (ppm) (slice 2), transpalatal suture (tps) (slice 3), and the palatal process of the palatine (ppp) (slice 4) levels (*n*=3 and 4 for control and cKO, respectively).

Figure 3. Mll4 is required for initial formation of the midpalatal suture prior to birth. (A–D) Skeletal staining (A, B) and trichrome staining results (C, D). Bone is stained magenta (in A, B) or blue (in C, D). The overall skeletal patterning was similar between the control (A, C) and *Mll4*-cKO palate (B, D) prior to birth (at E18.5). However, specifically in the newly established midpalatal suture (arrowheads in A, B; brackets in C′, D′), *Mll4*-cKO mice (D, D′) showed wider suture width, compared to the control mice (C, C′). (E–G, E′, F′) TUNEL staining revealed that *Mll4* deficiency resulted in significant increase in cell apoptosis in the midpalatal suture (brackets in E, F, E′, F′; G) (*n*=3 and 3 for control and cKO, respectively).

Figure 4. Mll4 regulates expression of genes associated with cartilage development in the newborn midpalatal suture. (A–D) Genome-wide mRNA expression analysis was performed using the control and *Mll4*-cKO midpalatal suture tissues at birth (P0.5). (A) Volcano plot, showing that total 117 genes were differentially expressed (p-value ≤ 0.001, log2FC ≥ 0.4)—40 upregulated genes and 77 downregulated genes. (B–D) Top 10-enriched biological processes (B) and heatmap (C), identified through Gene Ontology (GO) analysis from a list of significantly downregulated genes in the *Mll4*-cKO group, compared to the control group (D).

Figure 5. Mll4 is essential for timely differentiation of chondrogenic cells in the midpalatal suture at birth. (A–D) Immunofluorescence staining for expression of osteochondroprogenitor markers Col2a1, Sox9, and Runx2, as well as Mll4, in the control (A, C) and *Mll4*-cKO midpalatal suture (B, D) at birth (P0.5): Chondrogenic markers, Col2a1 and Sox9, are markedly reduced in the *Mll4*-cKO midpalatal suture (B1, D2), compared to control (A1, C2). In contrast, osteogenic marker, Runx2, showed similar expression in the control and *Mll4*-cKO suture tissue (A2, B2). Mll4 was markedly decreased in the *Mll4*-cKO palate (D1), compared to control (C1). Brackets (in A–D) indicate the midpalatal suture.

Figure 6. Mll4 is required for proper development of the midpalatal suture during postnatal palatogenesis. (A–J, I′, J′) Trichrome staining of the midpalatal suture in the control and *Mll4*-cKO mice, showing that *Mll4* deficiency results in significant retardation in the postnatal development of the midpalatal suture cartilage. (A, B) After birth (P0.75), the bilateral cartilage layers become present in the control midpalatal suture (A, arrowheads) but absent in the *Mll4*-cKO midpalatal suture (B). (C, D) At 1 week, the bilateral midpalatal suture cartilage layers become closer to each other and show uniform enlargement of the chondrocyte cells in the control mice (C, arrowheads), whereas the suture cartilage layers just start to partially appear in the *Mll4*-cKO mice (D, arrowheads). (E–J) At 3 weeks, the bilateral suture cartilage layers adhere to each other in the midline in both the control and *Mll4*-cKO midpalatal sutures, but the *Mll4*-cKO suture (F) is wider than the control suture (E), which becomes more obvious at 6 and 10 weeks (G–J). (I, J, I′, J′) At 10 weeks, the control suture cartilage remains present and narrow (I), and its chondrocytes are well differentiated

and organized (I′), whereas the *Mll4*-cKO midpalatal suture cartilage remains wide (J), and its chondrocytes are under-differentiated and disorganized (J′). Brackets (in A–J) indicate the midpalatal suture.

Figure 7. *Mll4* is essential for proper growth of the palate during postnatal palatogenesis. (A–D) Lateral growth of the palate was examined in the control and *Mll4*-cKO mice at 1, 3, 6, and 10 weeks. Horizontal length of the palate skeleton in the virtual coronal/frontal micro-CT sections was measured at the four representative levels: the incisive foramen (A), first molar (M1) (B), second molar (M2) (C), and third molar (M3) levels (D). *n*=6 for each of control and cKO at each of 1, 3, 6, and 10 weeks.

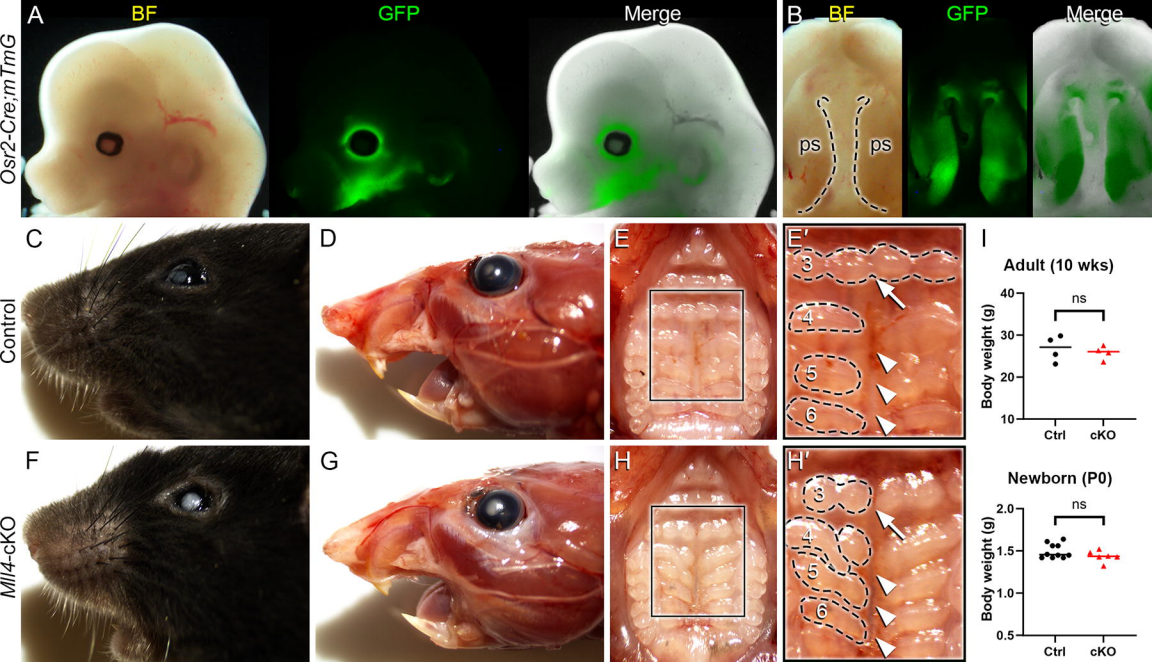
A
BF
GFP
Merge
B
BF
GFP
Merge
ps
ps
Osr2-Cre;mTmG
C
D
E
E'
3
4
5
6
I
Adult (10 wks)
ns
Body weight (g)
40
30
20
10
Ctrl
cKO
Control
F
G
H
H'
3
4
5
6
Newborn (P0)
ns
Body weight (g)
2.0
1.5
1.0
0.5
Ctrl
cKO
Mll4-cKO

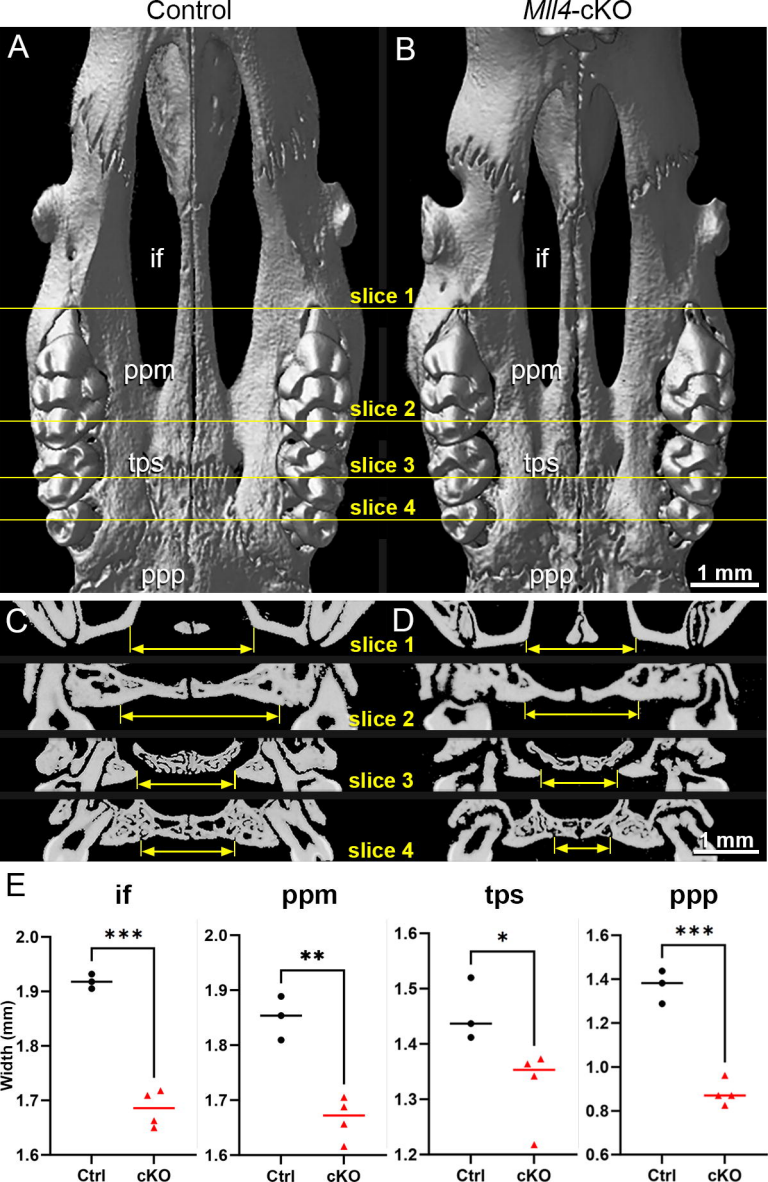
Control
Mll4-cKO
A
B
if
ppm
tps
ppp
slice 1
slice 2
slice 3
slice 4
1 mm
C
D
E
if
ppm
tps
ppp
Width (mm)
Ctrl
cKO
***
**
*
***

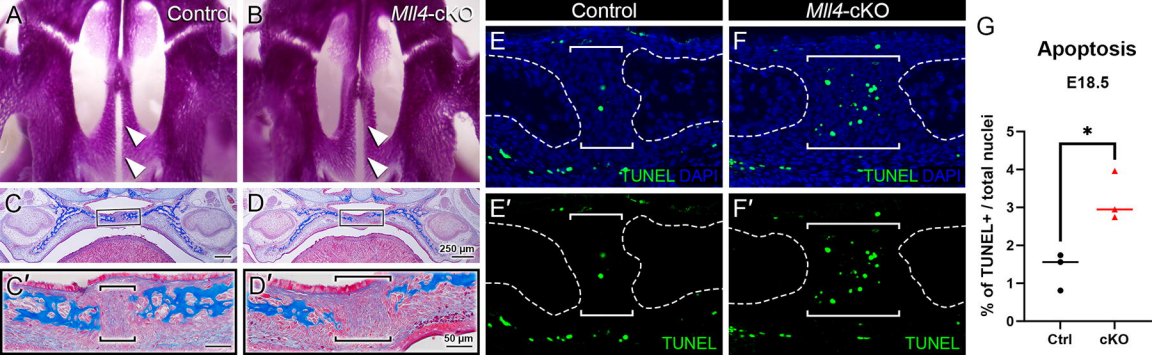
A
Control
B
Mll4-cKO
C
D
250 μm
C′
D′
50 μm
Control
Mll4-cKO
E
F
TUNEL DAPI
TUNEL DAPI
E′
F′
TUNEL
TUNEL
G
Apoptosis
E18.5
% of TUNEL+ / total nuclei
0
1
2
3
4
5
*
Ctrl
cKO

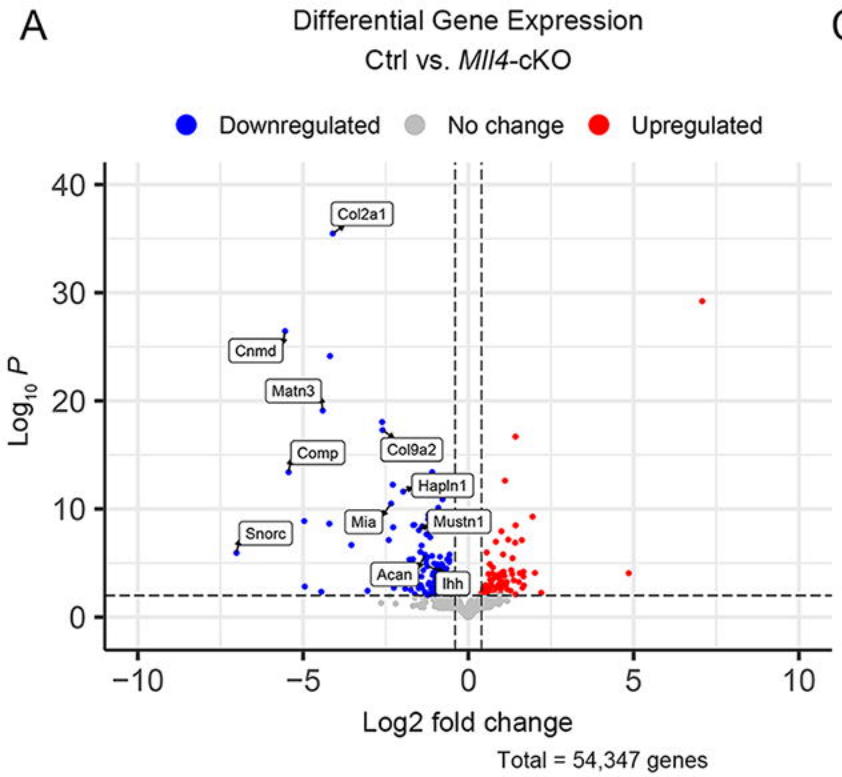

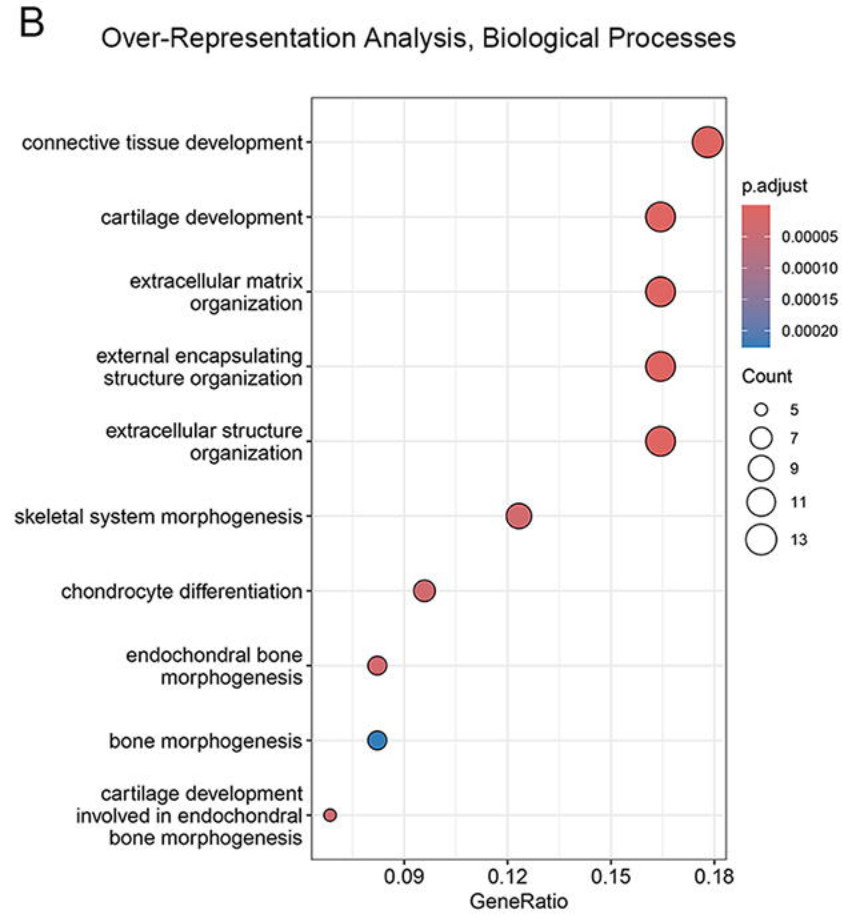

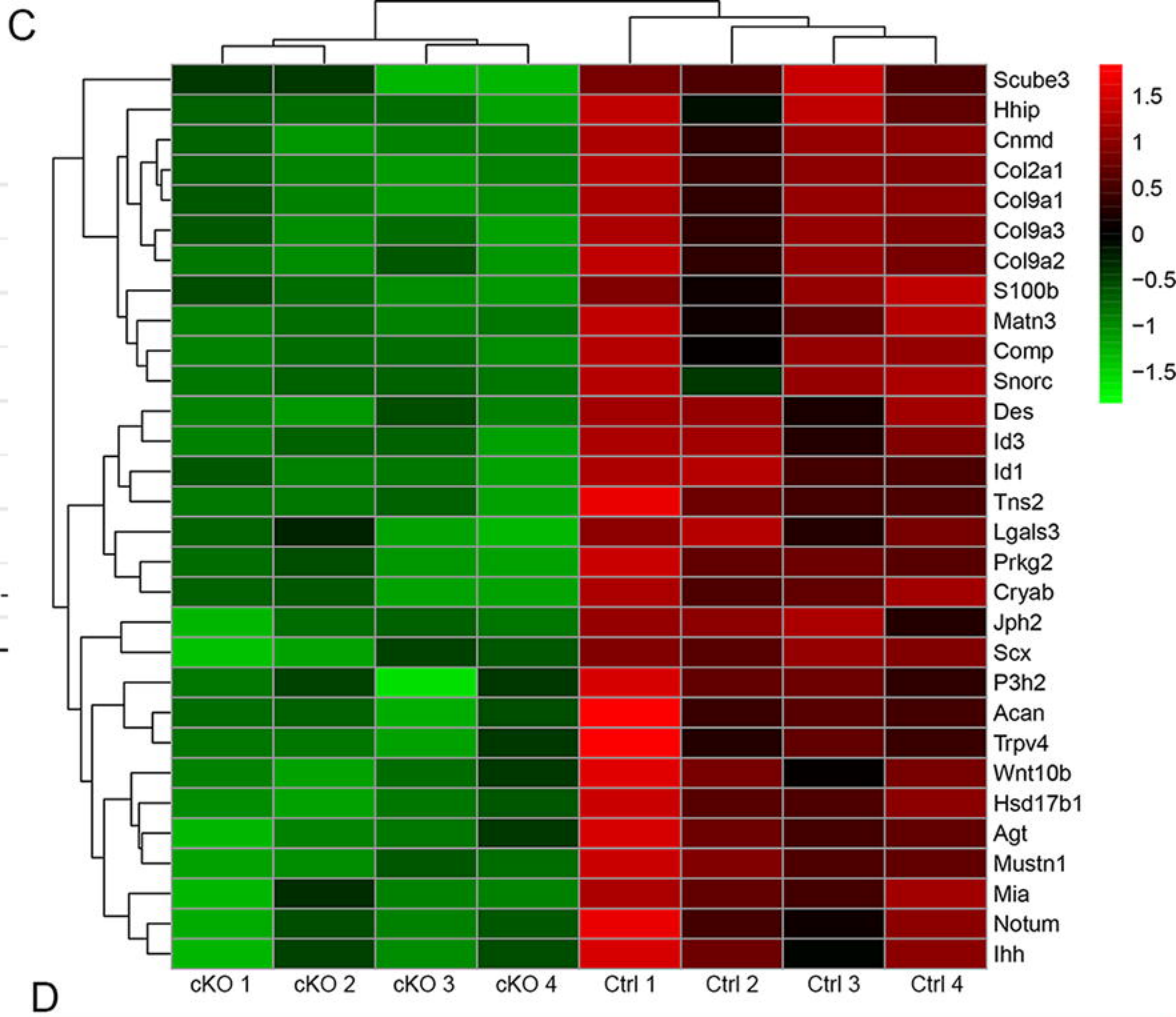

D

Description	Gene ID	Count
Cartilage development	Ihh, Trpv4, Matn3, Cnmd, Col2a1, Col9a1, Snorc, Prkg2, Acan, Comp, Scx, Mustn1	12
Connective tissue development	Ihh, Trpv4, Hsd17b1, Matn3, Cnmd, Col2a1, Col9a1, Snorc, Prkg2, Acan, Comp, Scx, Mustn1	13
Extracellular matrix organization	Ihh, Matn3, Col2a1, Col9a1, Col9a3, Col9a2, Acan, Comp, Agt, Scx, Lgals3, Mia	12
External encapsulating structure organization	Ihh, Matn3, Col2a1, Col9a1, Col9a3, Col9a2, Acan, Comp, Agt, Scx, Lgals3, Mia	12
Extracellular structure organization	Ihh, Matn3, Col2a1, Col9a1, Col9a3, Col9a2, Acan, Comp, Agt, Scx, Lgals3, Mia	12
Endochondral bone morphogenesis	Ihh, Trpv4, Col2a1, Col9a1, Comp, Scx	6
Chondrocyte differentiation	Ihh, Col2a1, Prkg2, Acan, Comp, Scx, Mustn1	7
Skeletal system morphogenesis	Ihh, Trpv4, Col2a1, Wnt10b, Col9a1, Acan, Comp, Scx, Hhip	9
Cartilage development involved in endochondral bone morphogenesis	Ihh, Trpv4, Col2a1, Col9a1, Comp	5
Bone morphogenesis	Ihh, Trpv4, Col2a1, Col9a1, Comp, Scx	6

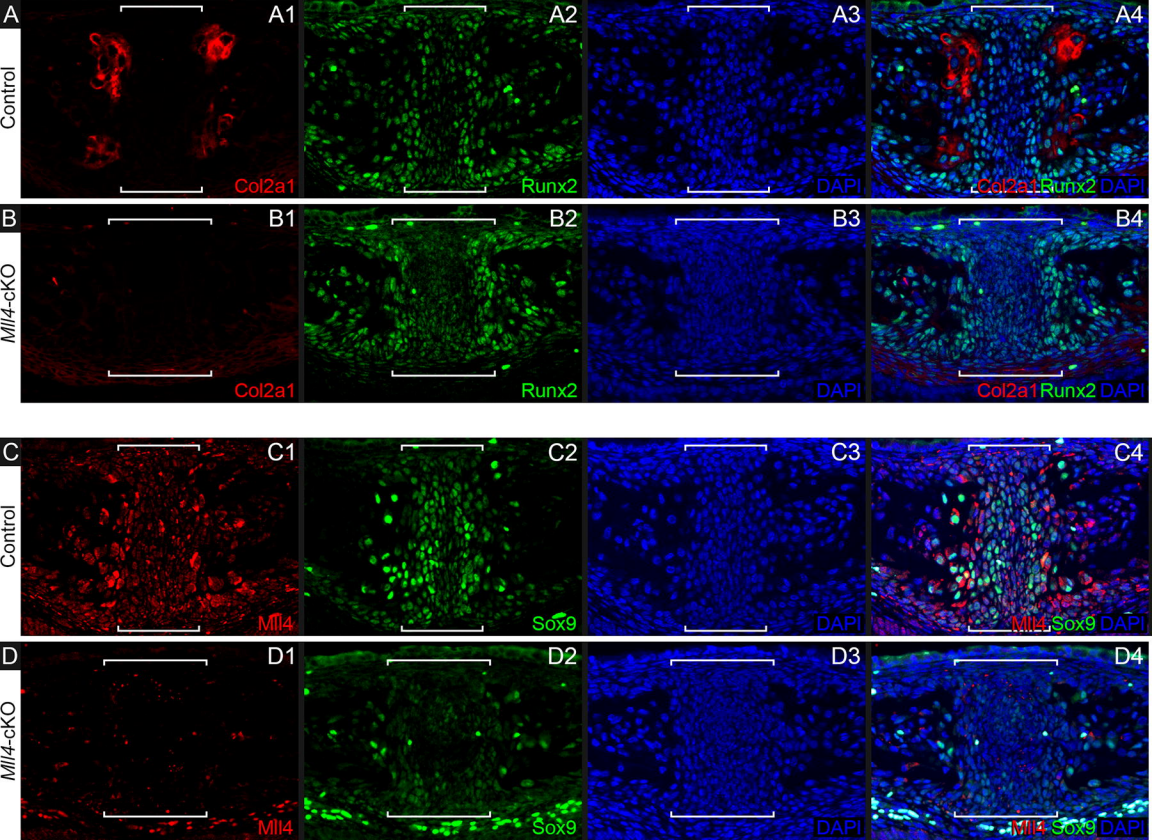
A
Control
A1
Col2a1
A2
Runx2
A3
DAPI
A4
Col2a1 Runx2 DAPI
B
Mll4-cKO
B1
Col2a1
B2
Runx2
B3
DAPI
B4
Col2a1 Runx2 DAPI
C
Control
C1
Mll4
C2
Sox9
C3
DAPI
C4
Mll4 Sox9 DAPI
D
Mll4-cKO
D1
Mll4
D2
Sox9
D3
DAPI
D4
Mll4 Sox9 DAPI

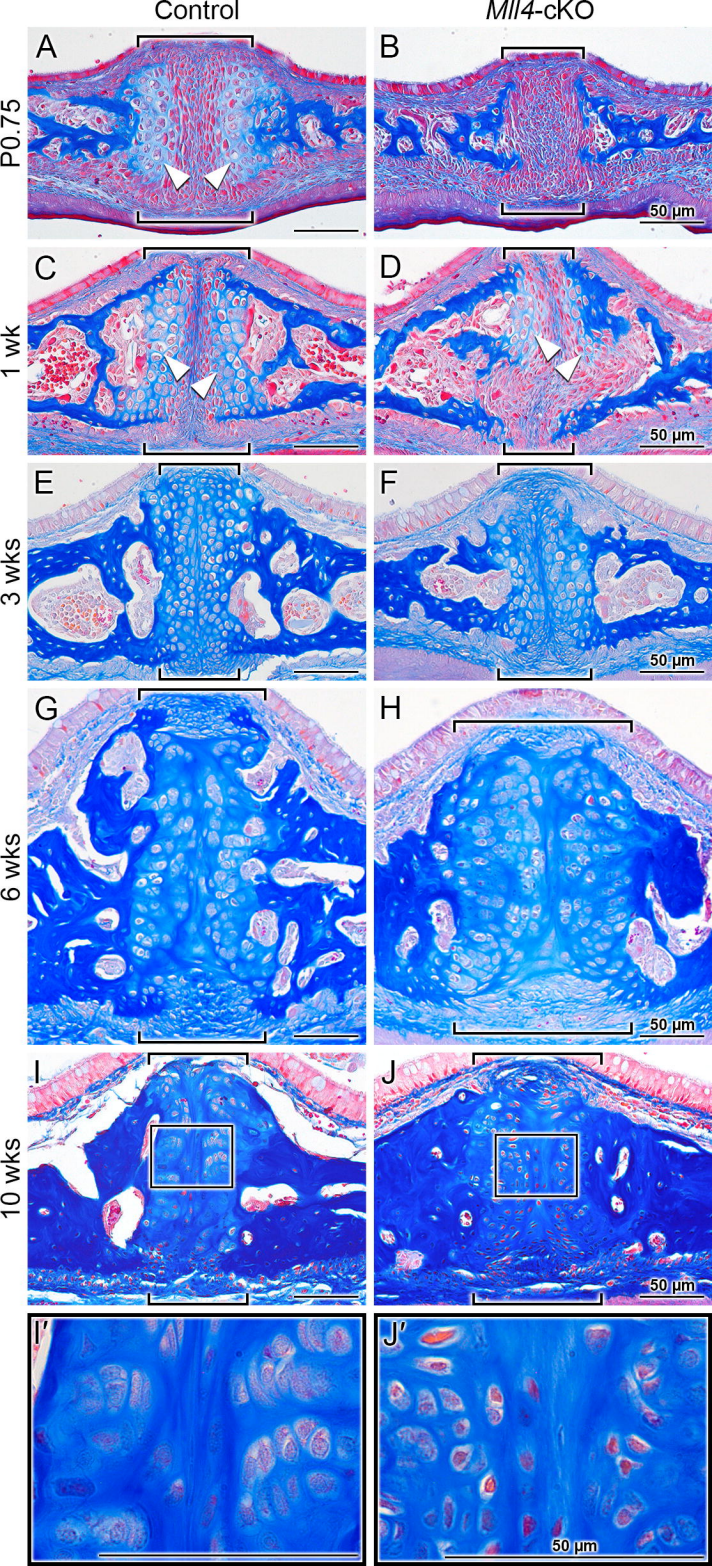
Control
Mll4-cKO
P0.75
1 wk
3 wks
6 wks
10 wks
A
B
C
D
E
F
G
H
I
J
I′
J′
50 μm
50 μm
50 μm
50 μm
50 μm
50 μm

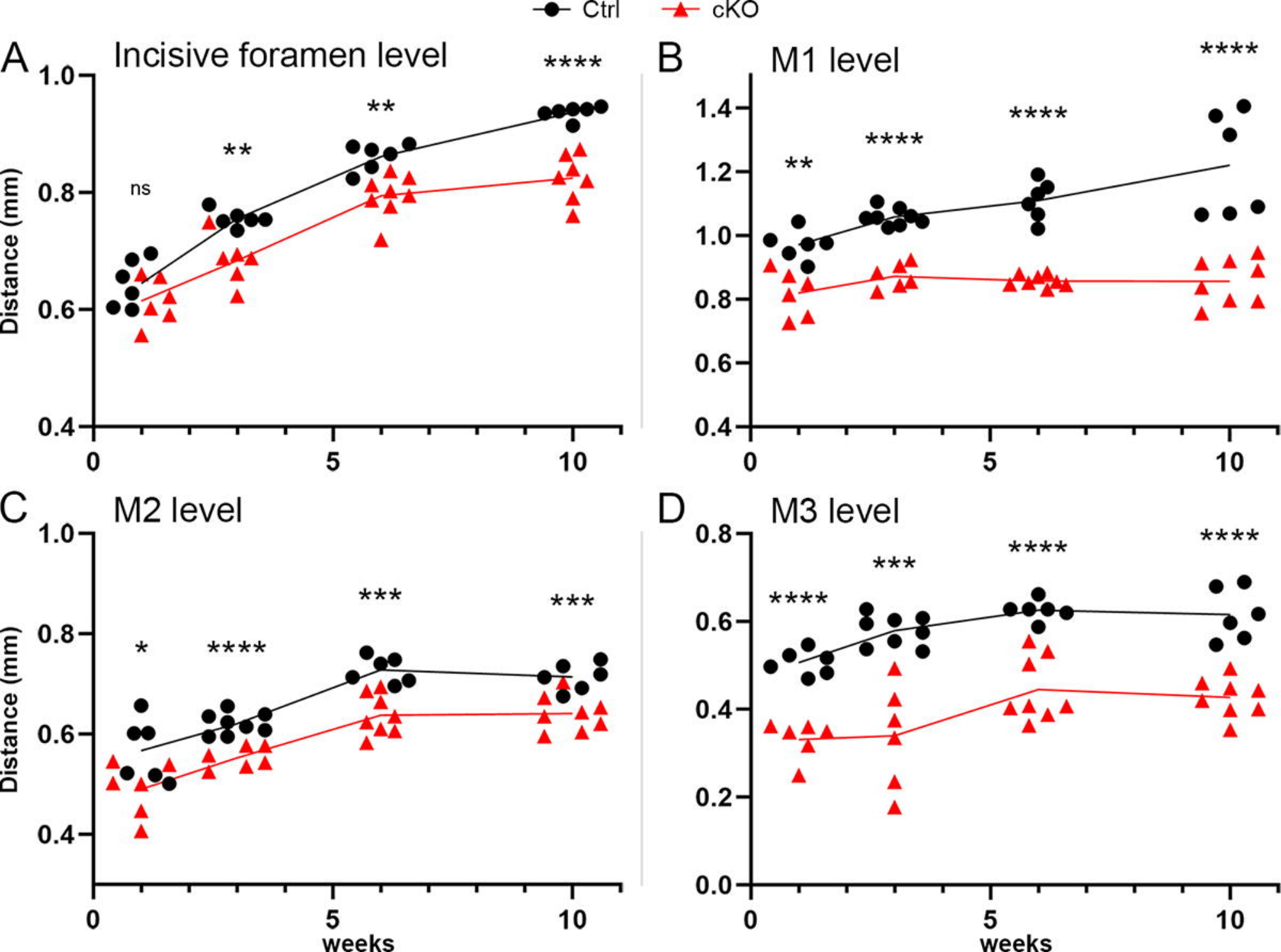
Ctrl
cKO
A
Incisive foramen level
Distance (mm)
ns
**
**
****
B
M1 level
**
****
****
****
C
M2 level
*
****
***
***
D
M3 level
****
***
****
****
weeks
weeks